Simulations of CO2-CO Infrared Radiation Measurements in Shock and Expansion-Tubes

Ulysse Dubuet, Satoshi Nomura, Shingo Matsuyama, Hiroki Takayanagi, Kazuhisa Fujita, Adrien Lemal

Simulations of CO_2-CO Infrared Radiation Measurements in Shock and Expansion-Tubes

Ulysse Dubuet[1]
Laboratoire EM2C, CNRS UPR288, CentraleSupélec, Université Paris-Saclay, 3 rue Joliot-Curie, 91190 Gif-sur-Yvette, France

Satoshi Nomura[2], Shingo Matsuyama[3]
JAXA, Chofu Aerospace Center, Tokyo, 182-8522, Japan

Hiroki Takayanagi[4], Kazuhisa Fujita[5]
JAXA, ISAS, Sagamihara, 252-5210, Japan

and

Adrien Lemal[6]
Astro Live Experiences Company Ltd., Tokyo, 107-0052, Japan

This paper presents the simulations of CO_2 and CO infrared radiation behind shock waves and in expansion flows. JAXA shock- and expansion-tube facilities were operated at conditions generating flow velocities ranging from 2.8 to 7.3 km.s^{-1}. Absolute infrared spectra of CO_2 and CO were obtained under equilibrium and nonequilibrium conditions and used to assess the performances of the spectral solvers and physico-chemical models. Specifically, this paper introduces the recent enhancements brought to JAXA in-house codes to compute CO_2 nonequilibrium infrared radiation. Schemes to split the level energy into its pure vibrational, rotational and vibration-rotation coupling, and interactions contributions were proposed and implemented. The correctness of the implementation was evaluated with comparison with literature data. Infrared radiation behind shock waves and under expansion regimes was analyzed with the newly developed model to infer the vibrational and rotational temperatures and determine the degree of thermal nonequilibrium.

[1] Research Assistant, laboratoire EM2C, CNRS UPR288, CentraleSupélec, Université Paris-Saclay, 3 rue Joliot Curie, 91190 Gif-sur-Yvette, France; ulysse.dubuet@student.ecp.fr, AIAA member.
[2] Researcher, Aeronautical Technology Directorate, Aerodynamic Research Unit, Chofu Aerospace Center, 7-44-1 Jindaiji-Higachi-Machi, Chofu, Tokyo 182-8522, Japan; nomura.satoshi2@jaxa.jp, AIAA member.
[3] Researcher, Aeronautical Technology Directorate, Numerical Simulation Research Unit, Chofu Aerospace Center, 7-44-1 Jindaiji-Higachi-Machi, Chofu, Tokyo 182-8522, Japan; matsuyama.shingo@jaxa.jp, AIAA member.
[4] Researcher, Research and Development Directorate, Research Unit II, Institute of Space and Astronautical Science, 3-1-1 Yoshinodai, Chuo, Sagamihara, Kanagawa 252-5210, Japan; takayanagi.hiroki@jaxa.jp. AIAA member.
[5] Professor, Department of Space Flight Systems, Institute of Space and Asrtonautical Science, Japane Aerospace Exploration Agency, 3-1-1 Yoshinodai, Chuo, Sagamihara, Kanagawa 252-5210, Japan; fujita.kazuhisa@jaxa.jp, Senior AIAA member.
[6] Chief Scientist, 2-21-1 Akasaka, Minato-ku, Kawamoto Building 2F, Tokyo 107-0052, Japan; adrien.lemal@gmail.com, AIAA member.

I. Nomenclature

a,b,c,d	=	powers of the *pseudo-temperature* $\tilde{T}$
C	=	Wang symmetry quantum number
d	=	CO_2 modal degeneracies, -
e	=	level energy, J
g	=	level degeneracy, -
H	=	effective Hamiltonian
h_p	=	Planck constant, $h_p = 6.62607004 \cdot 10^{-34}$ J.s
J	=	rotational quantum number
k_B	=	Boltzmann constant, $k_B = 1.38064852 \cdot 10^{-23}$J.K^{-1}
l_2	=	magnetic quantum number
N	=	state position in the *(P,J,C)* block
N	=	number density, m^{-3}
n	=	level population, m^{-3}
P	=	polyad quantum number
Q	=	partition function, -
T	=	temperature, K
v	=	vibrational level

Subscripts

i	=	CO_2 vibrational mode (i=1,2,3)
R	=	rotation
T	=	translation
V	=	vibration
v_1, v_2, v_3	=	vibrational quantum number of CO_2 vibration modes

II. Introduction

Upcoming missions to Mars considered by JAXA [1–3] generate strong motivation in designing advanced thermal protection systems (TPSs) with low design margins, in an effort to reduce the launching costs and increase the scientific value of the mission by embedding larger payloads and to enhance the reliability and safety of the reentry systems. The sizing of the TPSs relies on the knowledge of the physico-chemical processes heating the spacecraft on its front and back covers using a combined approach based on ground experiments and numerical simulations. For entries into CO_2-based atmospheres, measurements and simulations (reviewed in [4]) contributed to mitigate the uncertainties for the front shell of the TPS. The back shell received little attention since the heating loads, especially the radiative heating, were deemed negligible. However, recent numerical studies [1, 5–12] demonstrated that the radiative heating encountered by a spacecraft on its back shell was dominated by CO_2 infrared (IR) radiation (at 2.3, 2.7, 4.3 and 15μm) and was of the order of magnitude of the convective heating. These issues triggered experimental campaigns to characterize the radiation emitted under expansion conditions, which are deemed to be representative of afterbody heating conditions [13, 14]. Flight data were recently made available to the community [15-17] and used to assess the performances of the simulation models [18, 19]. Good agreement was obtained between predicted and measured radiative heat fluxes. However, this agreement was not conclusive on the accuracy of the kinetic and spectral models because of the lack of spatial or spectral resolution. These issues triggered additional measurement campaigns of CO_2 and CO IR radiation behind shock waves and during expansion. This paper aims at pursuing the experimental campaigns at flight representative conditions to enlarge the radiation database measurements and at upgrading the JAXA in-house physico-chemical models and solvers.

This paper is organized into three sections. Section III briefly describes the experimental facility, its sensors, flow and optical diagnostics used to measure the IR radiation from shocked and expansion flows. Section IV describes the computational framework developped to compute the IR radiation and focuses on the upgrades of the code developed in [4]. Section V discusses the results and assesses the performances of the solvers by comparing predicted and measured IR spectra for shocked and expansion flows.

III. Experimental setup

Experimental characterization of the flow surrounding a spacecraft is carried out in high-enthalpy facilities such as shock- and expansion-tubes. These high-enthalpy facilities were commissioned at JAXA Chofu Aerospace Center to support research in the aerothermochemistry of hypervelocity flight through Earth's and other planets' atmosphere (Mars, Venus, Gas Giants), as well as to simulate the high-enthalpy nonequilibrium phenomena encountered by spacecraft during atmosphere entry. JAXA facilities can work in shock-tube or expansion-tube modes to characterize the vibrational dynamics, kinetics and subsequent radiation from shocked and expansion flows and further characterize the radiation transferred to the front and afterbody of the spacecraft. The interested reader is referred to the works [13] where the facilities are thoroughly described.

The following sections briefly reminds the HVET facility outline, its sensors, as well as the flow and spatially and spectrally resolved emission spectroscopy diagnostics.

A. HVET Facility

The Hypervelocity Shock-tube (HVST) facility is a 16 m free-piston driven shock tube consisting of a reservoir tank, a compression tube, a high-pressure tube, a low- pressure tube, a vacuum tank, and a free piston, as depicted in Fig. 1. The 70 mm^2 cross section in the low-pressure tube is made of aluminum alloy to reduce the radiation emitted from impurities. Expansion of the flow is achieved with the adjunction of an aluminum vacuum chamber. High- and low-pressure tubes are evacuated down to 2~10 Pa with a turbomolecular pump and a dry pump before being filled with the gases. Two pressure transducers are mounted near the first and second diaphragms to measure the pressure evolution. The signal of the pressure transducer is monitored by digital oscilloscopes

The facility model comprises three sections: the compression tube (usually referred to as the driver tube), the high-pressure tube (usually referred to as the driven tube), and the low-pressure tube (where the expansion occurs). The sections are separated from each other by two diaphragms, D1 and D2.

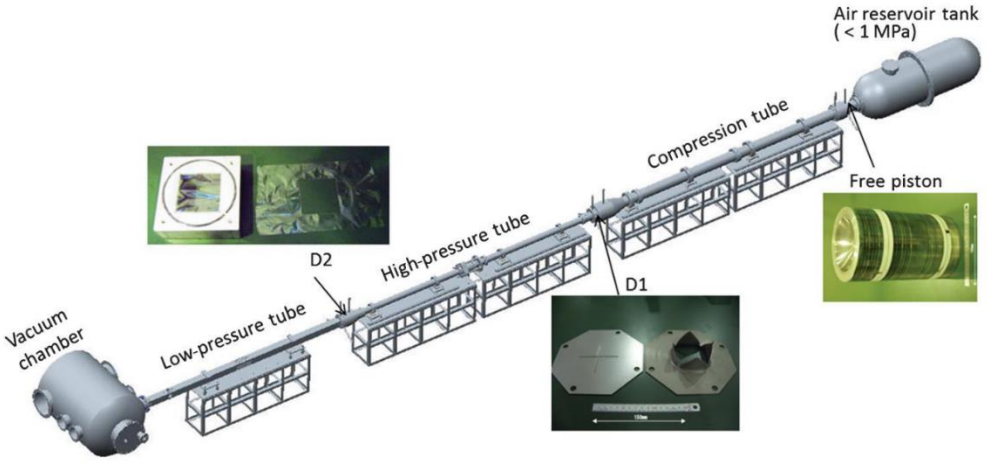

Fig. 1 HVET facility [13]

B. Flow Diagnostics

Pitot and static pressures were measured with various sensors. For pitot probe measurements, the pressure sensor was mounted in the 25-mm-diam probe inside a 1-mm-diam hole drilled at the tip of the pitot probe. The transducer was protected by a steel disk in order to protect it from the impact of the impurities. The static pressures were measured with two piezoelectric pressure sensors set at 25 and 125 mm upstream from the exit of the expansion section. The rise time of the pressure transducers was lower than 1 μs. The shock velocity was estimated, given the time elapsed between these transducer measurements. The uncertainties on the pressures and velocities were estimated with the standard deviation of the measured values.

C. Spatially and spectrally resolved optical diagnostics

Spatial distribution of IR radiation intensity through a Magnesium Fluoride (MgF_2) window was measured by a 640×512 medium-wavelength IR (MWIR) imager system. The sensors were kept at low temperature with liquid

nitrogen. The IR radiation was collected by a silicon planoconvex lens with a focal length of 200 mm. In front of the detector, a high-pass filter was added to reduce the emission from water vapor. The timing of the measurement was adjusted by a delay generator triggered by the pressure increase.

IR radiation spectra were obtained by the MWIR imager system set behind a Czerny-Turner asymmetric IR spectrometer with a focal length of 480 mm. Under shock-tube mode operation, the IR radiation spectra were collected at the position under investigation by an energy optimizer whereas, under expansion-tube mode operation, the IR radiation was collected by a light focus system with a sphere mirror. A high-pass filter was set in front of the entrance slit to reduce the high-order light. To eliminate the absorption by CO_2 and water vapor from ambient air, the IR spectrometer and the light focus system were purged with N_2 gas. The uncertainties on the radiation measurements were estimated of 30%

Wavelength calibration was accomplished by measuring the spectrum from an Hg source lamp at a high order of diffraction and by determining the reference wavelength position. The intensity calibration in the IR spectral range was achieved with a blackbody furnace of temperature T_B =1673 K.

D. Test conditions

To complement the shock-tube experiments performed in [20], an additional campaign was undertaken in HVST facility to measure the radiation behind shock waves travelling at speed ranging from 2 to 7 km.s^{-1} to fully characterize the radiance withstand by the front shield of a Martian spacecraft along various trajectories. The spectra measured in the 4.3µm were integrated along the line of sight perpendicularly to the shock-tube axis to yield the integrated radiance and compared with literature values from NASA Ames EAST facility [21], as illustrated in Fig. 2. As observed in Fig. 2, there is a good agreement between the integrated radiance from JAXA HVST and NASA EAST facilities both qualitatively and quantitatively. However, discrepancies occur at higher speed, since the radiation measurement from HVST are limited to 5.4µm and do not include the radiation from CO IR, as discussed in section V. Table 1 lists the operating conditions under consideration in this study.

Radiation measurements in expansion flows were previously undertaken in [13] to provide insight into the radiative heating withstand by the afterbody of a Martian spacecraft. Spectrally and spatially resolved measurement were obtained and complemented by Schlieren diagnostics. The interested reader is referred to [13] for further details.

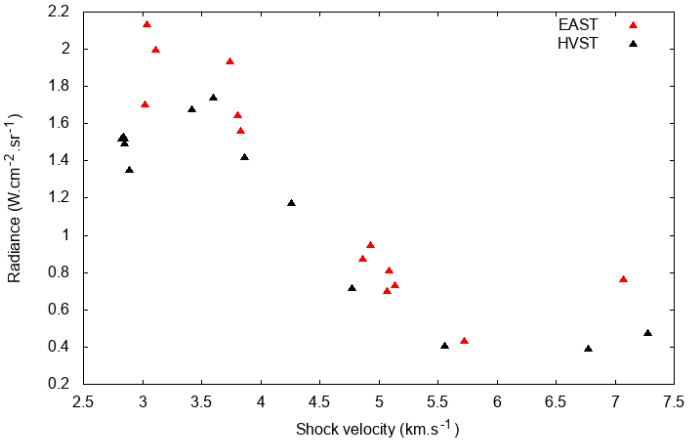

Fig. 2 Radiance comparison between JAXA HVST and NASA EAST [21] campaigns

Table 1 Operating conditions and thermodynamic state

Velocity, km.s^{-1}	2.84	2.85	2.89	2.82	2.85	3.42	3.60	3.87	4.77	4.26	5.56	6.77	7.27
Pressure, Pa	133.3 ± 0.1												

IV. Nonequilibrium spectral model

This section describes the computational tools and spectral models used to predict CO_2 and CO IR radiation. JAXA in-house Structured Package for Radiation Analysis (SPRADIAN) code [22] was upgraded [4] to include the Carbon Dioxide Spectroscopic Database (CDSD) [23, 24]. The performances of the solver were evaluated by comparing predicted and measured CO_2 IR radiation measurements under a comprehensive set of equilibrium conditions obtained from transmission cells, plasma torches and shock-tubes. CO radiation was previously included [1]. The purpose of the present work is to further upgrade the code to simulate nonequilibrium CO_2 IR radiation. The following sections derive rovibrational levels' energies and present the multi-temperature models used for nonequilibrium calculations.

A. Effective Hamiltonian

The present work considers the complete expression of the effective Hamiltonian to compute the rovibrational energy levels. The Hamiltonian is built using the same parameters, and the rovibrational levels' energy are obtained through its diagonalization.

Before diagonalization, it is possible to write the Hamiltonian as a sum of matrices, each one corresponding to a dynamic mode, coupling or interaction, as written in Eq. 1.

$$H_{eff} = H_{v_1} + H_{v_2} + H_{v_3} + H_{rot} + \widetilde{H} \tag{1}$$

where H_{v_i} corresponds to the *i*-th vibrational mode contribution, and $\widetilde{H}$ to the couplings and interactions. The H_{v_i} is composed of the terms using only $(v_i + d_i/2)$ in the diagonal terms of the Hamiltonian, as reminded in Eq. 2. [17].

$$\left(H_{v_i}\right)_{j,j} = \omega_i \left(v_i(j) + \frac{d_i}{2}\right) + x_{ii}\left(v_i(j) + \frac{d_i}{2}\right)^2 + y_{iii}\left(v_i(j) + \frac{d_i}{2}\right)^3 + z_{iiii}\left(v_i(j) + \frac{d_i}{2}\right)^4 \tag{2}$$

Denoting *P* the matrix of the change of basis for the diagonalization, the mode *mode* energy of the state $k = (P, J, C, N)$ is given by Eq. 3.

$$e_{k_{,mode}} = \left(P.H_{mode}.P^{-1}\right)_k \tag{3}$$

which is the *N*-th element on the diagonal in the (P, J, C) block of the diagonalized Hamiltonian. It is then possible to extract the contribution of each component to the rovibrational level's energy.

B. Populations

The population of a level $k = (P, J, C, N)$ under thermal nonequilibrium is given by Eq. 4.

$$n_k = \frac{N g_k}{\tilde{Q}} \exp\left(-\frac{e_{v_1}}{k_B T_{v_1}} - \frac{e_{v_2}}{k_B T_{v_2}} - \frac{e_{v_3}}{k_B T_{v_3}} - \frac{e_{\text{rot}}}{k_B T_{\text{rot}}} - \frac{\tilde{e}}{k_B \tilde{T}}\right) \tag{4.a}$$

$$\tilde{Q} = \sum_k g_k \exp\left(-\frac{e_{v_1}}{k_B T_{v_1}} - \frac{e_{v_2}}{k_B T_{v_2}} - \frac{e_{v_3}}{k_B T_{v_3}} - \frac{e_{\text{rot}}}{k_B T_{\text{rot}}} - \frac{\tilde{e}}{k_B \tilde{T}}\right) \tag{4.b}$$

$$e_k = e_{v_1} + e_{v_2} + e_{v_3} + e_{\text{rot}} + \tilde{e} \tag{4.c}$$

where e_{v_i} is the energy of the *i*-th vibrational mode (as explained in Section A), $\tilde{e}$ the energy of the couplings and different interactions, $\tilde{Q}$ the partition function and $\tilde{T}$ a *pseudo-temperature*. With the *(P,J,C,N)* labelling, the degeneracy of the vibrational modes is 1: thus $g_k = (2J + 1)/\sigma$, where σ is the symmetry number (equal to 2 in the case of CO_2) [25].

A database of approximately 7.3M states has been computed: this corresponds to a maximum polyad number *P* of 40, a maximum rotational number *J* of 300, and a cutoff energy of 55000cm^{-1}.

C. Multi-temperature model

For thermal nonequilibrium CO_2 flow, the choice of the *pseudo-temperature* $\tilde{T}$ arises. Inspired by Park's multi-temperature model [26], the expression shown in Eq.5 is proposed. This expression allows to explore different possibilities, and to add the coupling term to any mode or to a combination of the modes.

$$\tilde{T} = T_{v_1}^{a} T_{v_2}^{b} T_{v_3}^{c} T_{\text{rot}}^{d} \text{ where } a + b + c + d = 1 \quad (5)$$

V. Results

A. Implementation of the database

First calculations were made at equilibrium, for 4 different temperatures (1000, 2000, 3000 and 4000K) around 2.7 and 4.3µm, with a pressure of 1 atm and 100% of CO_2. A rectangular slit function of 10cm^{-1} has been applied to the spectra, in order to compare with Depraz's results [27]. The results for the 2.7µm band are plotted under the label SPRADIAN in Fig. 3. The "*Depraz – EM2C*" curve corresponds to the results obtained by Depraz in his thesis with the EM2C database, and shown in Fig. III.49 of [27].

A correct agreement with CDSD for all temperatures and spectral range considered is observed, and better than [27]. Nevertheless, for 2000K, Depraz's results are better than SPRADIAN's. This is the only case where SPRADIAN's results do not fit the best with CDSD. Some discrepancies still exist between SPRADIAN's results and CDSD in the other cases, but less than between CDSD and Depraz's results.

These good agreements allow to think that the calculated rovibrational levels' energies are correct and allow a good representation of the various levels. This also confirms that the modifications of SPRADIAN were successful. The rovibrational levels' energy database will thus be used for the next simulations presented in this paper.

Nevertheless, some improvements can still be made. The larger differences observed for higher temperatures suggest that the calculation of the higher levels' energies may not be the most accurate and could be improved.

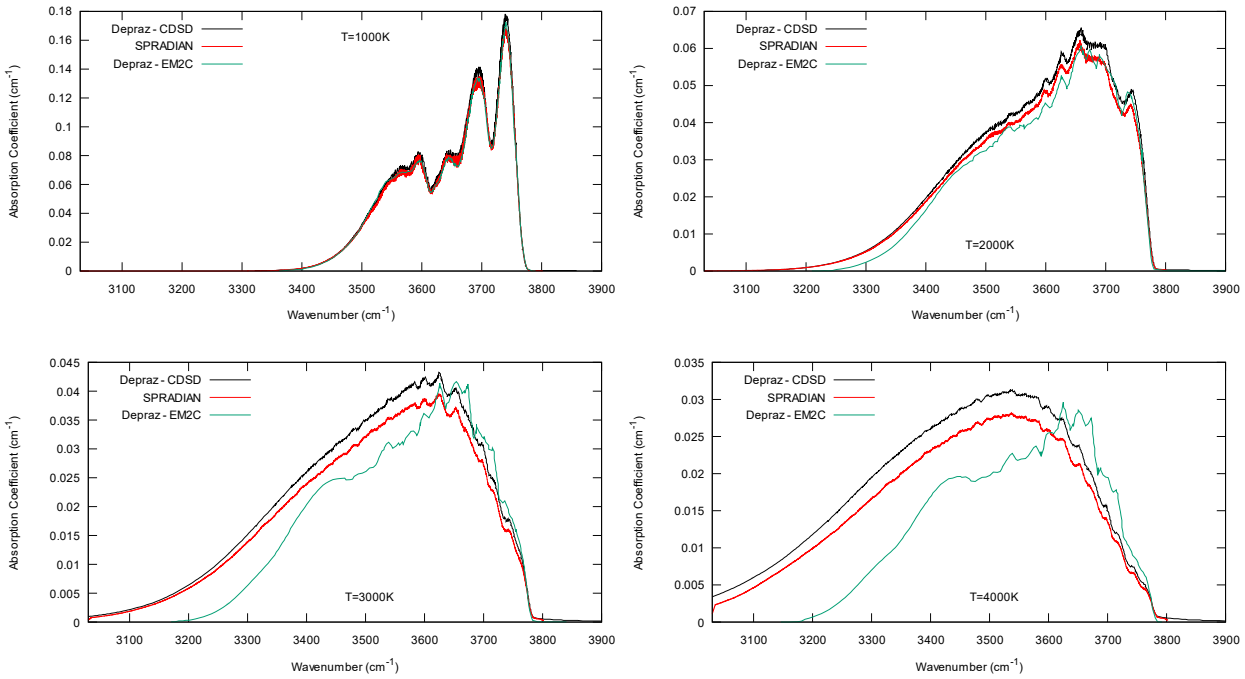

Fig. 3 Comparison of absorption coefficients at equilibrium.

B. Shocked equilibrium flows

The spectrally resolved radiance are shown in Fig. 4, and compared to simulations made with SPRADIAN for CO_2 and CO contributions. The mole fractions were obtained by the code Chemical Equilibrium with Application (CEA) [28], for frozen and equilibrium chemistries. For velocities lower than 4 km.s^{-1}, the radiation comes essentially from CO_2, and the radiation from CO can neglected. For case a), the chemistry is frozen (x_{CO2} = 1), for b), x_{co2} = 0.9 and for c), x_{CO2} = 0.25. For cases d), e) and f), the chemistry is at equilibrium. We observe that for higher shock velocities, the chemistry of the mixture gets closer to the chemical equilibrium. The equilibrium is reached for shock velocities higher than 5 km.s^{-1}, and CO radiation becomes predominant. This follows the observations made in [21] with EAST data.

In the case c), we tried to fit the experimental data using only CO_2 radiation, and were able to get an approached radiance for a pressure $p = 0.51$ bar and $x_{CO_2} = 0.25$ for a temperature of 4500K. Nevertheless, this can not represent the reality of the emitted spectra, since we have not computed CO emission, which would compensate the deficit in radiance after 5 μm. It is thus likely that the mole fraction of CO_2 will be lower than here (but larger than the equilibrium one), as well as its temperature, while CO will have a mole fraction lower than the equilibrium one. The mixture composition and governing parameters are listed in Table 2.

For higher temperatures (i.e. higher shock velocities), CO_2 dissociation rates increase and thus the chemical equilibrium is reached faster.

Table 2 Simulation parameters

	x_{CO_2}	x_{CO}	T_{eq} (K)	P (bar)
Case a)	1	0	$T_{frozen} = 3350$K	0.178
Case b)	0.9	0	4000	0.254
Case c)*	$1.051 \cdot 10^{-1}$	$5.204 \cdot 10^{-1}$	3400	0.518
Case d)	$1.769 \cdot 10^{-2}$	$5.153 \cdot 10^{-1}$	5000	0.693
Case e)	$6.974 \cdot 10^{-5}$	$4.289 \cdot 10^{-1}$	6500	1.014
Case f)	$4.204 \cdot 10^{-5}$	$3.536 \cdot 10^{-1}$	6900	1.172

* The parameters listed for case c) in this table correspond to the chemical equilibrium for a 4.77 km.s^{-1} shock. They result in the blue dotted curve in Fig. 4.

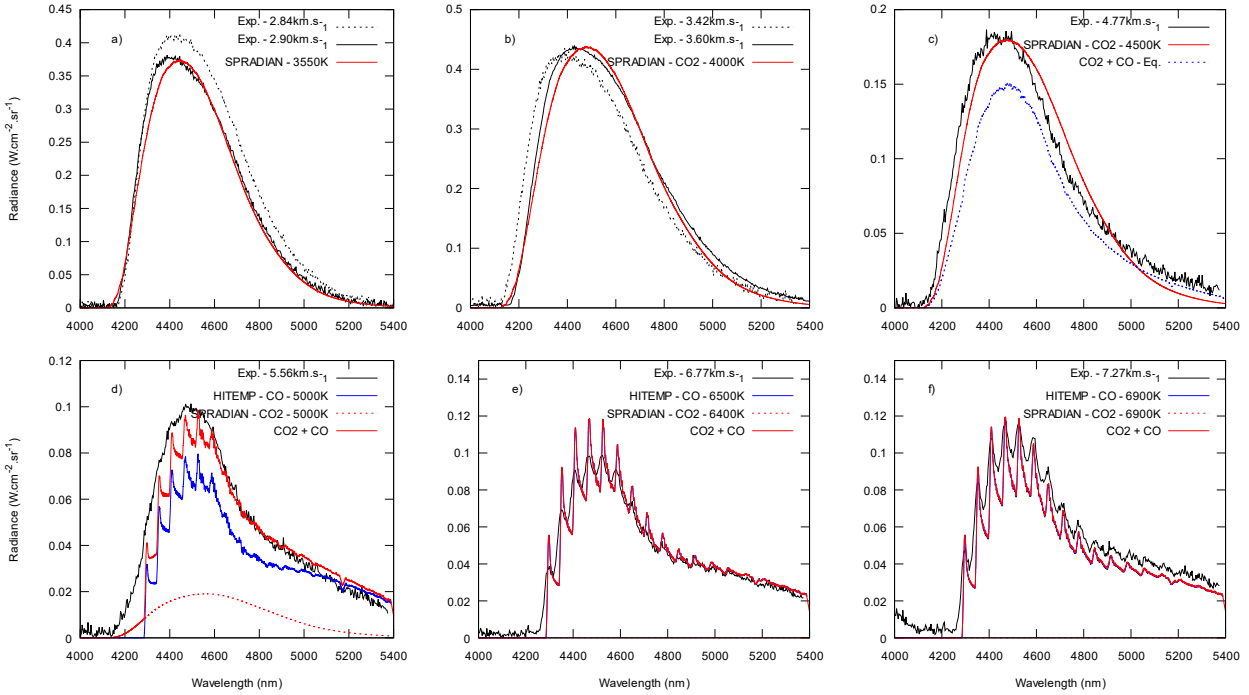

Fig. 4 Comparison between predicted and measured CO_2-CO IR spectra

C. Expanded nonequilibrium flows

Measurements were also performed with JAXA HVET facility [13]. The simulations of these measurements were previously performed at JAXA. As the article was written in Japanese, the strategy is described hereafter. Firstly, the flow was computed with JAXA in-house 2D axisymmetric CFD code JONATHAN [29]. Thermal nonequilibrium was described by Park model [21]. The flow variables perpendicularly to the tube axis were then extracted with an in-house ray-tracing program [30] and rotated around the tube axis. Subsequently, the flow variables were extracted along the measured lines of sight, as displayed in Fig. 5. The flow variables were then inputted into Ecole Centrale-Supélec radiation transport code [31]. The spectral properties were computed with the SNB model. As the SNB model

provided to the authors was working under equilibrium conditions, the spectra were computed at both the translational and vibrational temperature to bound the performances of the simulations.
Fig. 6 compares the predicted and measured spectrum. Fair agreement is observed between the simulations and the experimental data, while it is believed that upgrades of the physico-chemical models (kinetics and nonequilibrium radiation) are warranted.

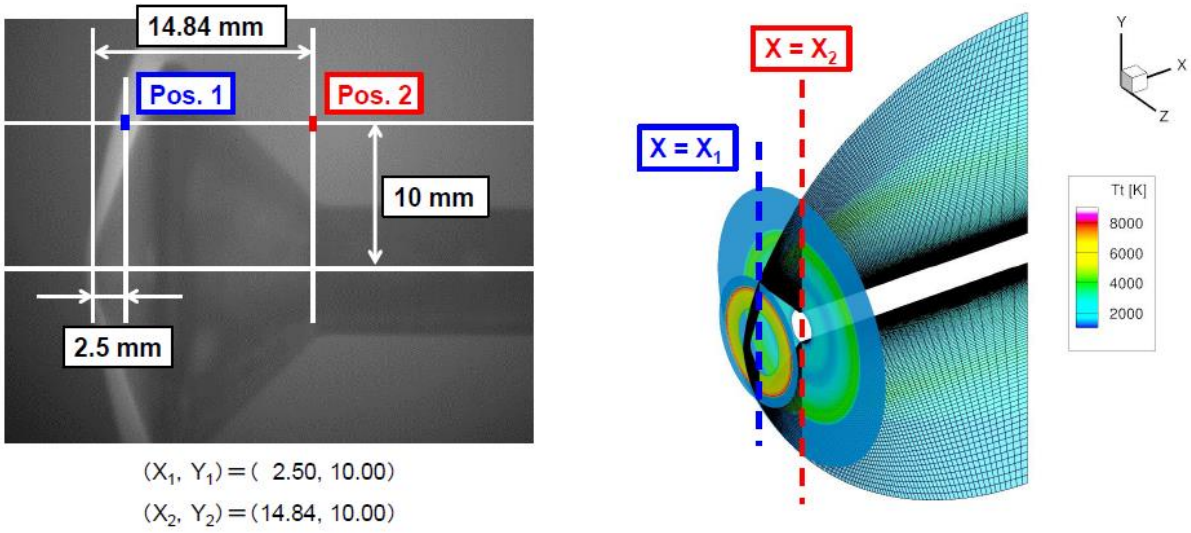

Fig. 5 Simulations of HVET line of sight flow [30, 31]

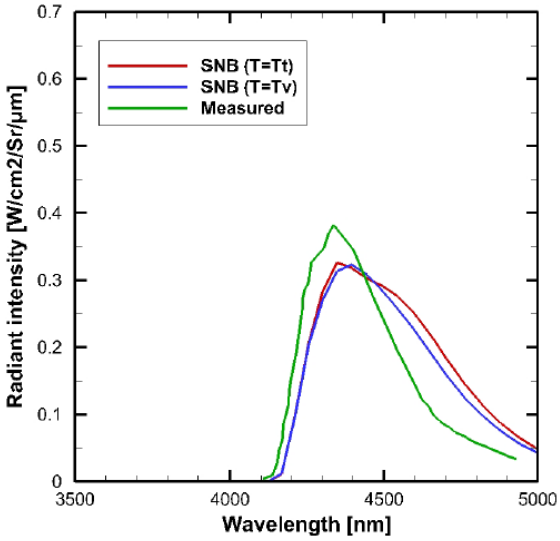

Fig. 6 Comparison between predicted and measured CO_2 IR spectrum (position 1) [30, 31]

Detailed studies on CO_2 vibrational dynamics remain necessary and the HVET measurement were used to test the performances of the spectral models and gain insight on nonequilibrium conditions. For example, Pannier and Laux used their recently developed code RADIS [32] to fit the experimental spectra [33]. The present work pursued the same approach and fitted the measured spectra to gain insight on CO_2 vibrational dynamics.

First simulations were performed using the same parameters as in [33]. The results are shown in Fig. 7. Correct agreement is found with RADIS's results (top figure), but a second set (bottom figure) simulations gives even better agreement with the experimental data. The RADIS curve corresponds to the best fit in [33], i.e. for T_r=1700K and T_v=2200K. SPRADIAN and RADIS fitting conditions are thus slightly different, but the same conclusion can be made: the vibrational temperature is twice smaller than the one predicted by Park's 2-temperature model (4000K). The

vibrational modes would thus relax quicker than the 2-temperature model predictions, which triggers an update of Park model for CO_2-based flows.

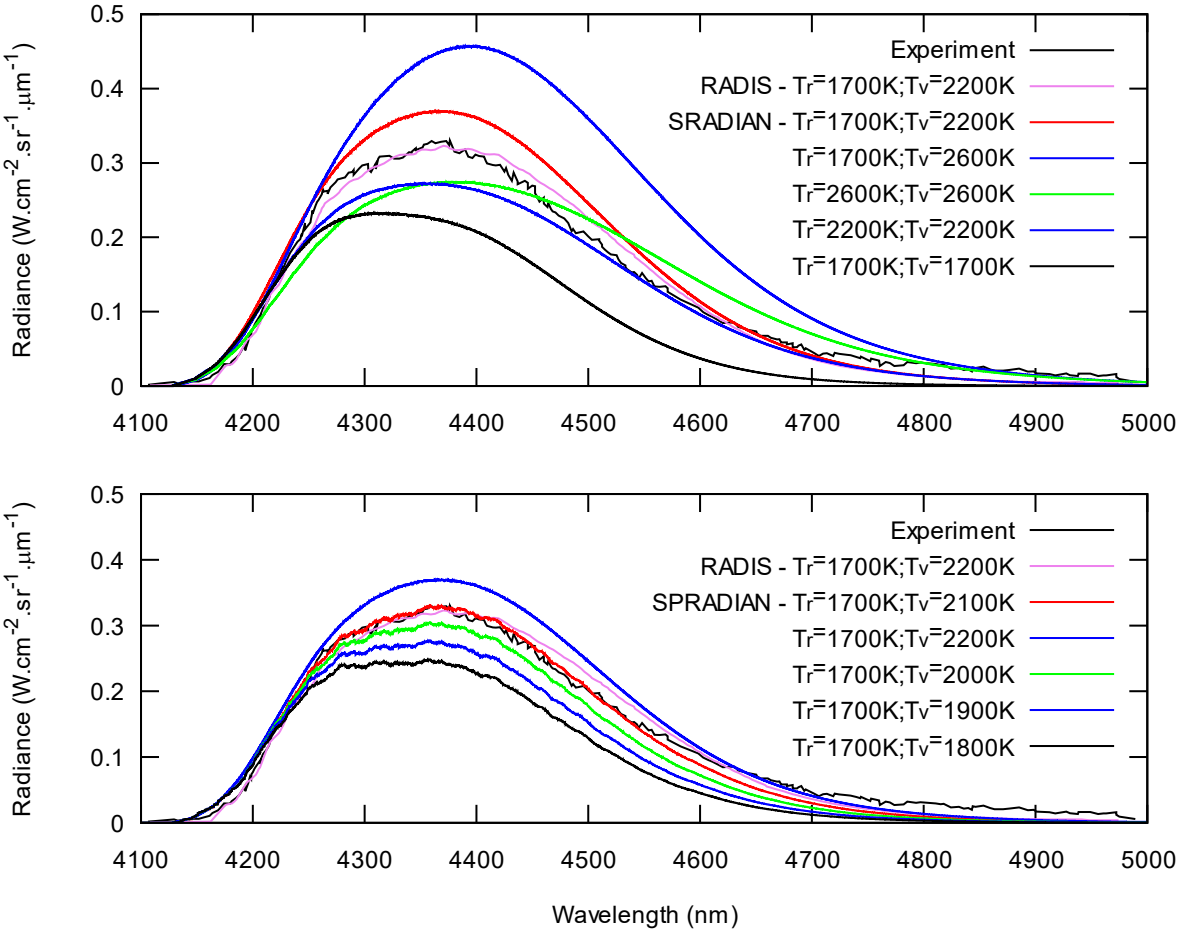

Fig. 7 Vibrational and rotational temperatures during expansion (free-flow) with parameters of [33] (top) and updated parameters (bottom).

VI. Conclusion

This paper presented the improvements to JAXA in-house radiation solver to compute CO_2 IR radiation under thermal nonequilibrium. The contributions of the couplings, interactions as well as the accurate computation of the energy levels were undertaken. Thermal nonequilibrium was described under the multi-temperature formalism. The implementation was evaluated with respect to previous works found in the literature.

To further validate the modeling, JAXA shock- and expansion-tube facilities were operated at conditions generating flow velocities ranging from 2 to 7 km.s^{-1}. Absolute spectral measurements were obtained in the 4.3 microns region and integrated to yield absolute radiances. The latter were compared to the measurements obtained at NASA EAST facility and good agreement was obtained. For shock velocities greater than 5 km.s^{-1}, the flow reaches chemical equilibrium, and CO IR radiation dominates CO_2 radiation.

The experimental spectra were analyzed with the model to determine the vibrational and rotational temperatures and determine the degree of nonequilibrium. Specifically, the measurements obtained during expansion confirms the nonequilibrium between vibrational and rotational temperatures. The relaxation times were found different from the predictions using the Park 2-temperatures model.

Acknowledgments

Thanks are due to Pr. C. O. Laux and Dr. E. Pannier (Ecole Centrale-Supélec, France) for their advices in the calculation of CO_2 rovibrational energies. Thanks are due to Dr. P. Riviere (CNRS, France) for providing the parameters of his SNB model and useful guidance. The improvements of the radiative solver were made thanks to a collaboration agreement between CNRS and JAXA. Thanks are due to JAXA and EM2C administrative staff for making this agreement possible.

References

[1] K. Fujita, S. Matsuyama, and T. Suzuki, "Prediction of Forebody and Aftbody Heat Transfer Rate for Mars Aerocapture Demonstrator," AIAA paper 2012-2001, 2012.

[2] S. Matsuyama, A. Lemal and K. Fujita, "Numerical Simulation of Flowfield Around Entry Capsule Using Multi-temperature Models" (in Japanese), 29th Shock Wave Symposium, Sendai, Japan, March 8th-10th 2018.

[3] K. Fujita et al., "Conceptual Study of Mars Aerocapture Orbiter for Engineering Demonstration and Science Observation", 32nd and 9th ISTS conference, Fukui, Japan, 2019.

[4] A. Lemal, H. Takayanagi, S. Nomura, and K. Fujita, "Simulations of Carbon-Dioxide Equilibrium Infrared Radiation Measurements," *J. Thermophys. Heat Transf.*, vol. 32, no. 1, pp. 184–195, 2017.

[5] A. M. Brandis, D. A. Saunders, C. O. Johnston, B. A. Cruden, and T. R. White, "Radiative Heating on the After-Body of Martian Entry Vehicles," AIAA paper 2015-3111, 2015.

[6] K. T. Edquist, B. R. Hollis, C. O. Johnston, D. Bose, T. R. White, and M. Mahzari, "Mars Science Laboratory Heat Shield Aerothermodynamics: Design and Reconstruction," *J. Spacecr. Rockets*, vol. 51, no. 4, pp. 1106–1124, 2014.

[7] M. Lino da Silva, P. Omaly and S. Surzhikov, "Contribution of CO_2 IR Radiation to Martian Entries Radiative Wall Fluxes," AIAA paper 2011-135, 2011.

[8] D. F. Potter, S. Karl, M. Lambert, and K. Hannemann, "Computation of radiative and convective contributions to Viking afterbody heating," AIAA paper 2013-20195, 2013.

[9] O. Rouzaud, L. Tesse, T. Soubrie, A. Soufiani, P. Riviere, and D. Zeitoun, "Influence of radiative heating on a Martian orbiter," *J. Thermophys. Heat Transf.*, vol. 22, no. 1, pp. 10–19, 2008.

[10] S. Surzhikov, "Radiative Gas Dynamics of MSL at Angle of Attack," AIAA paper 2016-, 2016.

[11] S. T. Surzhikov, "Radiative gas dynamics of MSL at angle of attack," AIAA paper 2016-742, 2016.

[12] T. K. West, J. Theisinger, A. J. Brune, and C. O. Johnston, "Backshell Radiative Heating on Human-Scale Mars Entry Vehicles," AIAA paper 2017-4532, 2017.

[13] H. Takayanagi, A. Lemal, S. Nomura, and K. Fujita, "Measurements of carbon dioxide nonequilibrium infrared radiation in shocked and expanded flows," *J. Thermophys. Heat Transf.*, vol. 32, no. 2, pp. 483–492, 2018.

[14] S. Gu, "Mars Entry Afterbody Radiative Heating: An Experimental Study of Nonequilibrium CO_2 Expanding Flow", Ph. D thesis, The University of Queensland, Brisbane, Australia, 2017

[15] B. Cruden, A. Brandis, T. White, M. Mazhari and D. Bose, "Radiative Heating During Mars Science Laboratory Entry: Simulation, Ground Test, and Flight", *J. Thermophys. Heat Transf.*, vol. 30, no. 3, pp. 642–650, 2016.

[16] A. Guelhan, T. Thiele, F. Siebe, R. Kronen and T. Schleutker, " Aerothermal Measurements from the ExoMars Schiaparelli Capsule Entry", *J. Spacecrafts and Rockets*, vol. 56, no. 1, pp. 68-81, 2019.

[17] G. Pinaud et al., "ExoMars 2016: A preliminary post-flight study of the entry module heat shield interactions with the martian atmosphere", 15th IPPW conference, Boulder, Colorado, US, 2018

[18] P. Boubert et al., "Rebuilding of ICOTOM radiometer data during Schiaparelli Martian entry", 8th RHTG workshop, Madrid, Spain, 2019.

[19] A. Brandis et al., "Reconstruction Of Schiaparelli And Comars Flight Data", 16th IPPW conference, Oxford, UK, 2019.

[20] H. Takayanagi and K. Fujita, " Infrared Radiation Measurement behind Shock Wave inMars Simulant Gas for Aerocapture Missions", AIAA paper 2014-198, 2014.

[21] B. A. Cruden, D. K. Prabhu, and A. M. Brandis, "Measurement and characterization of mid-wave infrared radiation in CO_2 shocks", AIAA paper 2014-2962.

[22] K. Fujita and T. Abe, "SPRADIAN, Structured Package for Radiation Analysis:Theory and Application," JAXA TR 669, 1997 (in Japanese).

[23] S. A. Tashkun, V. I. Perevalov, J. L. Teffo, L. S. Rothman, and V. G. Tyuterev, "Global Fitting of 12C16O2 Vibrational–Rotational Line Positions Using the Effective Hamiltonian Approach," *J. Quant. Spectrosc.*

Radiat. Transf., vol. 60, no. 5, pp. 785–801, 1998.
[24] S. A. Tashkun and V. I. Perevalov, "CDSD-4000: High-resolution, high-temperature carbon dioxide spectroscopic databank," *J. Quant. Spectrosc. Radiat. Transf.*, vol. 112, no. 9, pp. 1403–1410, 2011.
[25] G. Herzberg, *Molecular Spectra and Molecular Structure. II. Infrared and Raman Spectra of Polyatomic Molecules*. 1964.
[26] C. Park, J. T. Howe, R. L. Jaffe, and G. V. Candler, "Review of Chemical-Kinetic Problems of Future NASA Missions II- Mars entries.", *J. Thermophys. Heat Transf.*, vol. 8, no. 1, pp. 9–23, 1994.
[27] S. Depraz, "Etude expérimentale et modélisation des propriétés radiatives des mélanges gazeux de type CO_2-N_2 à très haute température en vue de l'application aux rentrées atmosphériques martiennes," Ph.D thesis, Ecole Centrale, Paris, France, 2014.
[28] B. J. McBride and S. Gordon, "Chemical Equilibrium with Applications." 1992.
[29] K. Fujita et al, "Development of JAXA Optimized Nonequilibrium Aerothermodynamics Analysis Code", JAXA TR 915, Tokyo, 2009 (in Japanese).",
[30] Y. Higuchi, M. Sc. thesis, University of Tokyo, 2018.
[31] P. Riviere and A. Soufiani, "Updated band model parameters for H_2O, CO_2, CH_4 and CO radiation at high temperature", Int. J. of Heat and Mass Transfer, vol. 55, no 13–14, pp. 3349–3358, 2012.
[32] E. Pannier and C. O. Laux, "RADIS : A Nonequilibrium Line- by-Line Radiative Code for CO_2 and HITRAN-like database species," *J. Quant. Spectrosc. Radiat. Transf.*, pp. 1–35, 2018.
[33] E. Pannier and C. O. Laux, "Analysis of the JAXA nonequilibrium infrared emission spectra for Mars entry conditions," 2019.
doi: 10.2514/1.T5646